Synthesis, spectra (FT-IR, NMR) investigations, DFT study, *in silico* ADMET and Molecular docking analysis of 2-amino-4-(4-aminophenyl)thiophene-3-carbonitrile as a potential anti-tubercular agent

Queen S. Obu [a,b], Hitler Louis [a,b,**], Joseph O. Odey [a,b], Ishegbe Joyce Eko [c,*], Shuaibu Abdullahi [d], Tabe N. Ntui [e], Ofiong E. Offiong [b]

[a] *Computational and Bio-Simulation Research Group, Department of Pure and Applied Chemistry, University of Calabar, Calabar, Nigeria*
[b] *Department of Pure and Applied Chemistry, Faculty of Physical Sciences, University of Calabar, Calabar, Nigeria*
[c] *Polymer and Textile Engineering, Ahmadu Bello University, Zaria, Kaduna, Nigeria*
[d] *Modibbo Adama University of Technology, Yola, Nigeria*
[e] *Department of Chemistry, Cross River University of Science and Technology, Calabar, Nigeria*

ARTICLE INFO

ABSTRACT

The title compound 2-amino-4-(4-aminophenyl)thiophene-3-carbonitrile (**AI3**), was synthesized and characterized experimentally by FT-IR, NMR and theoretically by quantum chemical calculations. The results were compared and the analysis of the results showed mutual agreement between the experimental and theoretical data. The theoretical calculations were performed using Density Functional Theory (DFT) method, Becke-3-Parameter-Lee-Yang-Parr (B3LYP) in $6-311++G$ (d,p) basis set. The Non Linear Optics (NLO), Natural Bond Orbital (NBO) including chemical reactivity parameters; Fukui function, Mulliken Population Analysis (MPA), Atomic Dipole Moment Corrected Hirshfeld (ADCH) population methods and the Natural Population Analysis were evaluated using the same level of theory. The results of the 3 population methods, MPA, NPA and ADCH were compared to examine charge distribution in the molecule. The Frontier Molecular Orbital indicated high bioactivity and NLO effects of the compound with a reduced value of the energy gap (-4.608103 eV) of the HOMO/LUMO which is also relatively comparable to its counterparts in the $+1/-1$ and $+2/-2$ states. The entire chemical reactivity analysis revealed C4 and N21 among the high donor atoms, then, S5 and C1 among the best acceptor atoms and this correlates with the location of the HOMO and LUMO in the studied compound. In addition, the antitubercular activities of the title compound against 3 (three) *Mycobacterium tuberculosis* proteins; 1P44, 1P45 and 4TZK were investigated using molecular docking simulations and the results were compared to those of Isoniazid (a standard anti-tubercular drug). **AI3** showed greater binding affinities (-6.0, -3.9 and **-**7.2 kcal/mol) in comparison to the Isoniazid drug (-5.5, -3.8 and -5.6 kcal/mol) for each target protein. Furthermore, an *in silico* study was performed to predict absorption, distribution, metabolism, excretion and toxicity profiles (ADMET) of the studied compound. The results reveal good to moderate anti-tubercular activity of the studied compound.

1. Introduction

Sulfur heterocycles have been considered for its enormous activities in drug research due to the availability of unshared pairs of electrons and electronegativity difference in conjunction with cyclic molecular structures. It has also been noted to have a low toxicity profile and high medicinal value compared to nitrogen heterocycles which dominates research in the development of drugs [1]. Due to its high reactivity and volatility, sulfur heterocycles have been employed in chemical and pharmaceutical industries for diverse functions [2,3]. Thiophene; a simple five membered sulfur heterocycle is predominantly found in natural products and biologically active compounds. Its derivatives are essen-

* Corresponding author.
** Corresponding author at: Computational and Bio-Simulation Research Group, Department of Pure and Applied Chemistry, University of Calabar, Calabar, Nigeria.
E-mail address: louismuzong@gmail.com (H. Louis).

tially used for a number of functions across fields of material science (development of polymer semiconductor and light emitting diode), life sciences (agrochemicals) and pharmaceutical sciences (drug research/design) [4,5]. Considering the vast role of thiophene and its derivatives as antifungal, antibacterial and antioxidants [6] as well as the growing interest in the review of experimental chemical species using computational methods; this study was performed to investigate the antitubercular activities of 2-amino-4-(4-aminophenyl)thiophene-3-carbonitrile (thiophene derivative) against the pathogenic bacteria, *Mycobacterium tuberculosis.*

Mycobacterium tuberculosis, Mtb is the causative organism for Tuberculosis (TB). Regardless of the availability of various classes of drugs, Mtb continues to trend well above HIV/AIDS as a top infectious killer in the world, leading to approximately 4000 deaths daily [7]. With prolong use of these available drugs, pathogenic bacteria develop spontaneous gene mutations and become resistant to them [8]. Due to this, continuous research is being made to develop anti-resistant drugs with low toxicity and low cost of treatment [9]. The studied compound, 2-amino-4-(4-aminophenyl)thiophene-3-carbonitrile was synthesized experimentally and results of its vibrational frequency and NMR were compared with the theoretical analysis performed using computational methods. The computational approach employed in this study is the Density Functional Theory (DFT) calculations. The DFT calculation [10] is effective in the exploration of the connection between the geometric and electronic properties of a chemical compound and it provides comparative agreement of results with experimental data [11].

Herein, the DFT calculations were performed using the *B3LYP/6–311++G (d,p)* basis set. The experimental and theoretical results for the vibrational frequency analysis (FTIR) and Nuclear Magnetic Resonance (NMR) spectra analysis were reported. The energies of the Frontier Molecular Orbitals (FMO) involving the Highest Occupied Molecular Orbital (HOMO) and the Lowest Unoccupied Molecular Orbital (LUMO) were analyzed with tabular and graphical representations. Fukui functions, chemical reactivity descriptors, Natural Bond Orbital (NBO), Electrostatic Potential (ESP), and a comparison between 3 population analysis; MPA, NPA and ADCH were calculated and reported to reveal the most reactive sites in the compound and its overall reactivity. To check for drug potentiality, effectiveness and likeness, the ADMET analysis were performed as well as molecular docking simulations using various *Mycobacterium tuberculosis* target proteins, 1P44, 1P45 and 4TZK.

2. Method

2.1. Synthesis of 2-amino-4-(4-aminophenyl)thiophene-3-carbonitrile

P-aminoacetophenone (0.03 mol, 4.1 g) and malononitrile (0.06 mol, 3.96 g) were condensed in toluene using a heterocatalytic system. The reaction mixture was refluxed in the presence of catalytic amount of acetic acid and ammonium acetate to produce arylidenemalononitrile as an intermediate, followed by the cyclization with sulfur, using diethylamine as catalysts at 65°c for 3 h to give the desired products. The brownish crystalline product obtained was left to cool overnight. Thereafter, it was filtered, washed with ethanol, ethanol and water (1:1) and dried. The brownish yellow crystals were purified and recrystallized from hot ethanol (see Fig. 1 for the optimized geometry).

Where $R = C_6H_5NH_2$

Yield: 89%; Melting point: 186 °C; Molecular mass: 177 gmol^{-1}, Molecular formula: $C_{11}H_9N_3S$; *m/z*: 215.05 (100%), 216.06 (11.9%), 217.05 (4.5%), 216.05 (1.19%); Elemental analysis: C 61.37, H 4.21, N 19.52, S 14.89.
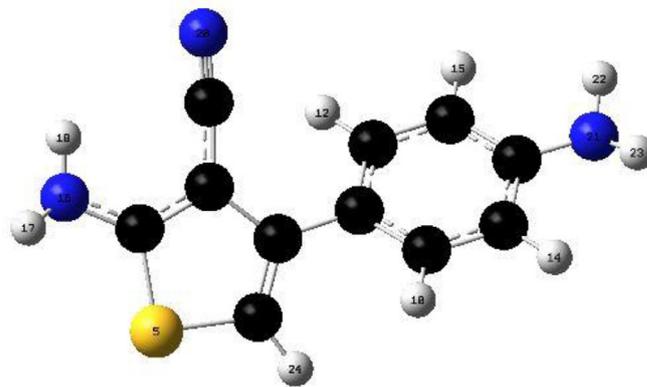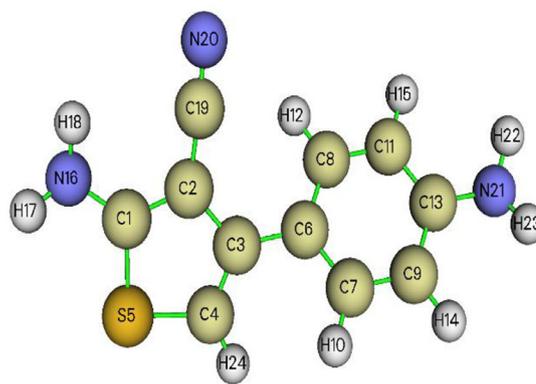

Fig. 1. Crystal and optimized structure of **AI3** with atoms numbering of compound and optimized structure.

2.2. Spectra details

The experimental Fourier Transform Infrared (FTIR) spectrum (**Fig. 2.**) was recorded using potassium bromide (KBr) disk at wavenumber region 4000–650 cm^{-1} with a CARY 630 FTIR–Agilent technology spectrophotometer and with a spectral resolution at 8cm^{-1}. ^{1}H NMR and ^{13}C NMR were obtained using Bruker AVANCE-III spectrometer and chemical shift (δ) values were recorded in parts per million (ppm).

2.3. Computational details

The Avogadro software [12] was used to draw the molecular structure of **AI3**. The compound's molecular geometry optimization was performed using the density functional theory at B3LYP level [13] with 6–311++G (d,p) with the aid of the Guassian 09 W software [14]. All geometries were visualized using GuassView 6 software package [15]. The nuclear magnetic resonance spectra (^{1}H and ^{13}C NMR) were obtained by using the gage-invariant atomic orbital (GIAO) method. The entire vibrational assignments of wave numbers were made on the basis of potential energy distribution (PED) by VEDA 4 program [15]. The dipole moment, mean polarizability, first order hyperpolarizability (nonlinear optical properties) and the fukui functions of **AI3** were computed with Guassian 09 W program. The ADCH population analysis and FT-IR spectra were computed with the aid of the Multiwfn anazlyzer [16,17].

2.4. Pharmacological investigation

The drug likeness based on Lipinski's rule of five (RO5) were determined for the studied compound using Molinspiration on-

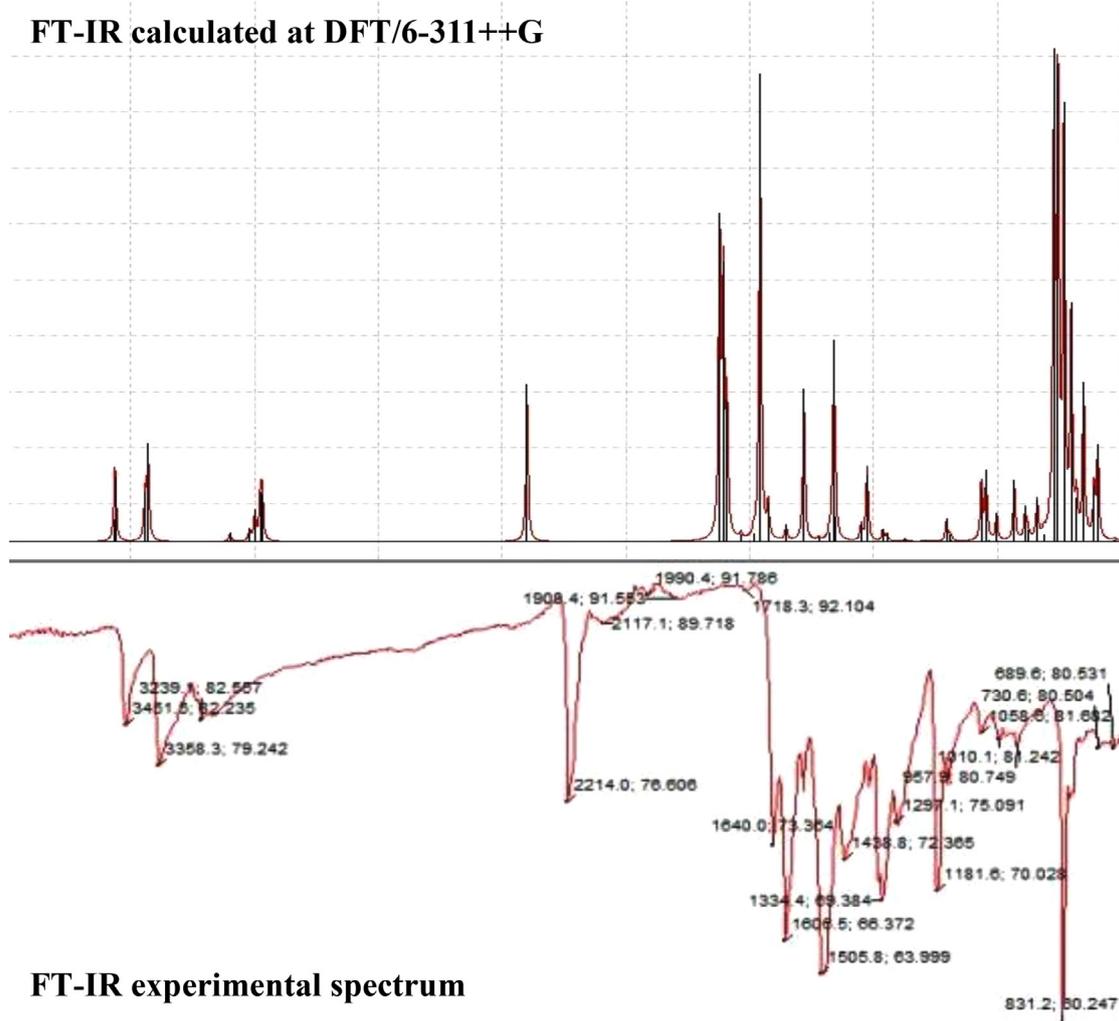**FT-IR calculated at DFT/6-311++G**

FT-IR experimental spectrum

Fig. 2. Theoretical and experimental infrared spectrum of 2-amino-4-(4-aminophenyl)thiophene-3-carbonitrile.

line server [18]. The ADMET properties were calculated using the pkCSM online server [19]. Cell permeability, penetration properties, carcinogenicity (toxicity) prediction in rat were determined. The molecular docking prototype was made on the AutoDockTools-1.5.6 [20]. The crystal structures of the protein, 1P44, 1P45 and 4TZK were obtained from the Protein Data Bank (www.rcsb.org) and the reference drug (Isoniazid) was downloaded from DRUGBANK (www.drugbank.com). The AutoDockTools were used to eliminate water molecules, co-crystalized ligands and to add polar hydrogen to the protein. The docking simulations were performed using the AutoDockVina format, thereafter, the pdbqt docked conformations were investigated using the Discovery Studio Visualizer. The preferred conformation was selected on the basis of their binding affinities.

3. Result and discussion

3.1. Spectral analysis

3.1.1. Vibrational analysis

Vibrational analysis provides information on the chemical compositions of samples through characteristic bands within specified range. In drug research/design, FT-IR spectra is employed in the evaluation of the type of polymorphism existing in a drug sub-

stance [21]. The nonlinear molecule has a total number of $3N-6$ modes, where N represents the number of atoms present in the molecule [22]. The studied compound consists of 24 atoms and 66 modes of vibrations. Out of the 66 normal modes were 23 stretching, 22 bending and 16 torsion modes. Also, 5 out-of-plane modes were observed. The spectral assignments along with the potential energy distributions (PED) are presented in **Table 1**. The experimental Fourier Transform Infrared (FTIR) spectrum **Fig. 2.** was recorded using potassium bromide (KBr) disk at wavenumber region 4000–650 cm^{-1} with a CARY 630 FTIR–Agilent technology spectrophotometer and the spectrum was recorded with a spectral resolution at 8cm^{-1} while the theoretical FTIR were calculated and plotted using the optimized structure output file on Multiwfn software application. In the result, the scale factor (0.96) was employed to give comparative theoretical and experimental wavenumbers.

3.1.2. N−H vibrations

In heterocyclic compounds, the N−H stretching vibration usually occur between 3500 and 3200 cm^{-1} [23]. The stretching N−H was observed experimentally at 3239cm^{-1}, 3358cm^{-1}, 3451cm^{-1} respectively. Theoretically, it was calculated as 3544, 3553, and 3652cm^{-1} also with an asymmetric stretching vibration at 3650cm^{-1}.

Table 1
Experimental and calculated frequencies of **AI3** at B3LYP method with 6−311++G (d,p) basis set.

Mode No.	Experimental IR (cm^{-1})	Calculated Frequency	I_{IR}	Assignments with PED%
3	3451	3652	2.83	νNH (100)
1		3650	1.42	ν_{asy}NH (98)
4	3358	3553	2.53	νNH (100)
2	3239	3544	3.99	νNH (98)
5		3279	2.67	νCH (99)
7		3215	3.89	νCH (94)
6		3198	9.27	νCH (83) + νCH (16)
9		3180	40.26	νCH (94)
6		3175	3.89	νCH (83) + νCH (83)
10	2224	2239	1.17	νNC (89) + ν_{asy}CC (10)
29		1697	12.54	βHNH (68) + τHNCC (10)
27		1685	16.04	βHNH (80)
17	1640	1673	24.79	ν_{asy}CC (49) + βHNH (16) + βHCC (15)
16	1606	1628	43.14	νCC (54)
11		1587	19.06	ν_{asy}CC (45) + βHCC (11)
11		1567	19.06	ν_{asy}CC (21) + νCC (10) + βHCC (26)
12		1540	2.32	νCC (63) + βHCC (11)
13		1482	1.37	νCC (34) + βHCC (36)
18		1425	70.89	νCC (37)
13		1482	1.37	νCC (18) + βHNC (15) + βHCC (45)
15		1341	0.43	νCC (21) + βHCC (24)
14		1328	0.66	νNC (64) + βHCC (16)
18		1322	70.89	νCC (12) + νNC (22) + νCC (12)
22		1239	212.97	νCC (16) + βHCS (39)
26	1334	1221	5.24	βHNC (16) + βHCC (41)
26		1220	5.24	βHNC (18) + βHCC (32)
13		1169	1.37	νCC (22) + βHNC (11) + βHCC (48)
18		1155	70.89	ν_{asy}CC (10) + νNC (13) + βHNC (15) + βHCS (26)
28		1098	27.46	βHNC (54)
33		1034	0.63	βHCC (15) + βCCC (66)
24		964	2.83	βCCC (21) + τHCCC (12)
51		952	208.86	τHCCC (60) + τHCCC (10)
52		947	3.34	τHCCC (72) + τCCCC (13)
20		851	106.59	ν_{asy}NC (10) + νSC (12) + βCCC (18)
20		849	106.59	ν_{asy}NC (25) + βCCC (20) + βCCC (18)
23	831	835	219.98	νSC (11) + τHCCC (49)
53		825	2.95	τHCCC (90)
23		802	219.98	νSC (12) + βCCC (24) + βCCC (10)
63		745	43.75	Out CCCC (71)
50		709	17.09	τHCSC (16) + τCCCC (43)
50		700	17.09	τHCSC (51) + Out NCSC (32)
21		671	196.02	νCC (16) + βCCC (10)
48		616	68.05	τHNCC (54)
47		604	1.51	τHNCC (36) + τCCCC (12)
38		585	1.41	βCCC (13) + τHNCC (14)
47		561	1.51	τHNCC (26) + τNCCC (23) + τCCCC (11)
23		544	219.98	ν_{asy}SC (17) + βCCC (36) + βSCC (10)
58		521	20.80	Out CCCC (48)
55		487	124.63	τNCCC (40) + Out NCSC (19) + Out CCCC (20)
23		475	219.98	νSC (10) + βSCC (39)
42		425	8.20	βCCN (35) + βCCC (17)
52		420	3.34	τHCCC (15) + τCCCC (77)
41		393	29.53	βCCN (52) + Out CCCC (13)
41		344	29.53	βCCN (16) + Out CCCC (47)
49		312	7.19	τHNCC (84)
42		305	8.20	βCCN (22) + βCCC (15) + τHNCC (13)
46		275	3.64	τHNCC (71)
22		269	212.97	ν_{asy}CC (24) + βCCC (13) + βCCC (22)
64		248	21.77	τCCCS (67)
66		192	9.71	Out CCCC (50)
40		139	5.49	βCCC (37) + βCCC (13) + Out CCCC (25)
40		124	5.49	βCCC (40)
44		82	10.82	βCCC (42) + τCCCC (11) + Out CCCC (13)
65		61	28.41	Out CCCC (65)
60		51	13.73	τCCCS (67)

ν - stretching.
ν_{asy}- asymmetric stretching.
β- in plane bending.
τ - torsion.
Out - out-of-plane.
Wavenumbers (in cm^{-1}) calculated at B3LYP/6−311++ G (d,p) using scaling factors 0.96.

Table 2
Comparison of *B3LYP/6–311++G (d,p)* calculated and experimental values of ^{13}C and ^{1}H chemical shift (ppm) relative to the TMS for **AI3**.

Atom	Experimental δ (ppm)	Theoretical δ (ppm) (B3LYP/ 6–311++G (d,p))
C1	28.5166	28.3436
C2	104.2695	104.8015
C3	54.1161	54.3781
C4	87.3607	87.1027
C6	71.4571	71.5501
C7	70.0135	67.2065
C8	65.8319	66.5979
C9	82.0619	82.5011
C11	82.0951	82.2981
C13	50.4001	51.2071
C19	85.4101	85.3341
H10	25.4652	25.1552
H12	22.8249	24.7419
H14	26.4184	25.9594
H15	24.0396	25.8466
H17	25.8211	28.9071
H18	28.6494	28.1794
H22	28.9961	29.5481
H23	29.9619	29.6279
H24	27.3585	26.6395

3.1.3. C≡N vibrations

The C≡N Nitrile group vibrations are usually recorded at 2260–2240cm^{-1} [24]. The studied compound showed a stretching vibration with a characteristic band experimentally at 2224cm^{-1} and was theoretically calculated as 2239 cm^{-1}.

3.1.4. C=C vibrations

The aromatic C=C bond are generally observed with a medium to weak absorption band at 1600 −1475cm^{-1} [24,25]. **AI3** showed a stretching vibration and medium absorption at 1640, 1606 and 1505cm^{-1}, it was theoretically calculated at 1673cm^{-1}, 1628cm^{-1} and 1540cm^{-1} respectively.

3.1.5. C−H vibrations

A bending vibration of C−H band corresponding to the CH$_3$ group on the phenyl ring was observed at 1334cm^{-1} experimentally and calculated as 1221cm^{-1}.

3.1.6. C-S vibrations

The C-S stretching vibration was observed at 831cm^{-1} and calculated as 835cm^{-1} theoretically [26].

3.1.7. Nuclear magnetic resonance

The understanding of basic levels of biomolecular structures are essential in drug research. NMR spectroscopy presents atomic-level structural information through identifying high affinity ligands for biologically relevant macromolecules and elucidating ligand-binding sites [27]. This was performed using ^{1}H NMR and ^{13}C NMR. The NMR analysis was carried out using chloroform (CDCl$_3$) as solvent and tetramethylsilane (TMS) as internal standard. In order to standardize the NMR spectra, the chemical shifts are positioned in relation to a reference proton set at 0.00 ppm. Tetramethylsilane (Si(CH$_3$)$_4$), is the standard for ^{1}H NMR. The corresponding spectra are represented in the supporting information as **Figs. S3. (a and b)** and **S4. (a and b)**. From the analysis, the experimental and theoretical ^{13}C NMR chemical shift values of the aromatic carbon lies within the range 50.4001–82.0951 and 51.2071–82.2981 respectively.

The **AI3** chemical shifts (**Table 2.**) at 28.5166, 104.2695, 54.1161, 87.3607 and 71.4571, 70.0135, 658,319, 82.0619, 82.0951, 50.4001 (ppm) correspond to signals for the various C−C bond of the thiophene and the phenyl ring respectively. The doublet calculated

at 50.4001 and 85.4101 ppm is attributed to the nitrogen on the C = N bond which shifted downfield. This is due to the inductive effect of the amino group both on the aminothiophene and on the phenyl ring. The high chemical shift 104 ppm observed at C2 is due to the cyano group it is attached to on the thiophene ring. The signal recorded experimentally as 28.5166 and 28.3436 theoretically (upfield) are associated the C atom attached to the NH group on the thiophene ring.

The ^{1}H NMR spectra of **AI3** indicates the singlet with a high deshielding effect at 29.9619 ppm (experimental) and 29.6279 ppm (theoretical) are attributed to H23 atom on the NH$_2$ group of the aromatic ring. The most shielded singlet is observed at H12 with 22.8249 ppm (experimental) and 24.7419 (theoretical). The ^{1}H NMR and ^{13}C NMR analysis observed, shows good correlation of results obtained both experimentally and theoretically.

3.2. Fukui functions

Fukui functions are chemical descriptors that identify atomic sites susceptible to electrophilic and nucleophilic attacks. The condensed Fukui functions and dual descriptor for the studied structure were calculated using Multiwfn in its N. $N + 1$ and N-1 electronic states respectively.

The condensed fukui function [28] is given as;

$$f^+ = q_N - q_{N+1} \text{(Nucleophilic attack)} \qquad (1)$$

$$f^- = q_{N-1} - q_N \text{(Electrophilic attack)} \qquad (2)$$

The condensed dual descriptor is given by; $\Delta f = f^+ - f^-$.

If $\Delta f > 0$, then the site is favored for nucleophilic attack. If $\Delta f < 0$, then the site is susceptible to an electrophilic attack. On this premise, the atomic sites susceptible to nucleophilic attack are in the order; S5 > C1 > N20 > C19 > H17 > C3 > C2 > H24 > H18 > C13. Consequently, the sites susceptible to electrophilic attack are as follows; C7 > H10 > H14 > H15 > C4 > H12 > C8 > N16 > C11 > C9 > C6 > N21. Although, it can be observed that the Δf of H22 and H23 values are <0, thus, they behave as nucleophiles. This nucleophilic behavior is as a result of the electron density around the nitrogen atom they are attached to. The Fukui functions and dual descriptors for all the atomic sites of the studied compound are tabulated in **Table S3.** of the supporting information.

3.3. Atomic charges

Atomic charges serve to describe the distribution of charges in a molecule. Its relevance stretches across the fields of molecular modeling and quantum chemistry. It provide details of electrostatic interactions with molecular force fields [29]. The atomic charges of the **AI3** are obtained by Mulliken Population Analysis (MPA), Natural Population Analysis (NPA) and the Atomic Dipole Moment Corrected Hirshfeld (ADCH) population methods. The ADCH population analysis is very efficient and not sensitive to basis set, however, the predicted charges from ADCH are generally smaller than those from Mulliken [30]. The MPA and NPA are sensitive to basis set; a change in basis set, induces a corresponding change in the calculated net charges. However, NPA gives better charge distributions because it is calculated based on the natural charges [26].

In this study, the ADCH charges were calculated using Multiwfn analyzer, while the MPA and NPA charges were extracted from the results of the Natural Bond Orbital (NBO) analysis which was performed using Guassian 09 W at *B3LYP 6–311++G (d,p)* basis set. The results obtained were compared to study the distribution of charges based on the different population methods in **Table 3.** From the result, the charges on N-atoms calculated by ADCH, MPA

Table 3
Comparison of Mulliken population analysis, natural population analysis and atomic charges for Structure performed at B3LYP method with 6–311++G (d,p) basis set.

Atoms	MPA Charges (e)	ADCH (e)	NPA charges (e)
C1	0.05456	−0.23501	0.05675
C2	0.09853	0.20206	−0.27028
C3	0.13664	0.12466	−0.03749
C4	−0.43679	−0.46412	−0.43878
S5	0.25004	0.25798	0.43473
C6	0.09294	0.03720	−0.09959
C7	−0.17758	−0.06009	−0.19415
C8	−0.17681	−0.40673	−0.19019
C9	−0.17846	−0.05439	−0.27875
H10	0.12910	0.06367	0.23629
C11	−0.17980	−0.13005	−0.27501
H12	0.14982	0.25419	0.24670
C13	0.32047	0.06430	0.17519
H14	0.11879	0.08418	0.23072
H15	0.12418	0.14739	0.23347
N16	−0.76070	−0.58300	−0.82705
H17	0.34403	0.35972	0.41274
H18	0.35604	0.34063	0.42308
C19	0.21703	0.16166	0.26932
N20	−0.51476	−0.38617	−0.33463
N21	−0.78917	−0.65644	−0.83020
H22	0.32355	0.34615	0.39811
H23	0.32184	0.34432	0.39693
H24	0.17650	0.18789	0.26209

Table 4
Occupancy of natural orbitals and hybrids of compound for C, H, N, S atoms.

Parameters	Occupancies (e)	Hybrids	Atomic Orbitals%
σ C1 - C2	1.96794	sp$^{1.47}$	s(40.54%)p(59.43%)d(0.03%)
σ C2 - C19	1.97600	sp$^{2.17}$	s(31.49%)p(68.46%)d(0.05%)
σ C4 - S5	1.97708	sp$^{3.01}$	s(24.94%)p(74.94%)d(0.13%)
σ C8 - H12	1.97952	sp$^{2.39}$	s(29.48%)p(70.47%)d(0.05%)
σ C13 - N21	1.99239	sp$^{2.51}$	s(28.47%)p(71.43%)d(0.10%)
σ N16 - H18	1.98267	sp$^{2.73}$	s(26.81%)p(73.13%)d(0.06%)
LP σ S5	1.98355	sp$^{0.55}$	s(64.45%)p(35.53%)d(0.02%)
LP σ N20	1.96899	sp$^{0.85}$	s(54.03%)p(45.91%)d(0.06%)
σ^* C1 - C2	0.02915	sp$^{1.47}$	s(40.54%)p(59.43%)d(0.03%)
σ^* C2 - C19	0.03311	sp$^{2.17}$	s(31.49%)p(68.46%)d(0.05%)
σ^* C4 - S5	0.01399	sp$^{3.01}$	s(24.94%)p(74.94%)d(0.13%)
σ^* C8 - H12	0.01200	sp$^{2.39}$	s(29.48%)p(70.47%)d(0.05%)
σ^* C13 - N21	0.01808	sp$^{2.51}$	s(28.47%)p(71.43%)d(0.10%)
σ^* N16 - H18	0.01056	sp$^{2.73}$	s(26.81%)p(73.13%)d(0.06%)

and NPA respectively, are negative. This is because nitrogen is more electronegative than the other atoms and can accepts electrons freely. The result also shows positive charges for all H atoms across all population analysis. This can be due to the surrounding electronegative nitrogen atoms. The C atoms have diverse negative and positive charges. The highest negative charge on the C atom is located on C4, while the highest positive charge is on C13 for MPA, C2 for ADCH and C19 for NPA. The S5 atom attached to the heteroatom has a net positive charge for all population analysis.

3.4. NBO analysis

The investigation of the natural bond orbitals offer details on the intra/inter molecular hydrogen bonding, conjugative interaction and the hyper conjugative interaction in a compound [31]. Here, the natural bond orbital analysis were performed using the Guassian 09 W application package at *B3LYP* density functional method with *6–311++G (d,p)* basis set. The corresponding donor-acceptor stabilization energy, $E^{(2)}(i \rightarrow j)$ for each donor (*i*) NBO and acceptor (*j*) NBO is given as;

$$E^{(2)} = q_i \frac{(F_{i,j})^2}{\varepsilon_j - \varepsilon_i}$$

Where *qi* is the orbital occupancy, *i, j* are diagonal elements and $F_{i,j}$ is the off-diagonal NBO Fock matrix element [32]. The greater extent of conjugation enjoyed by the molecular system is due to the larger values of the stabilization energy, E$^{(2)}$. The delocalization of electron density between a lone pair or bonding and Rydberg or antibonding NBO orbitals increases the stabilizing donor-acceptor interaction.

From the output of the NBO analysis, the total Lewis structure has 97.67% (core, 99.96% and valence Lewis, 96.49%) and the non-Lewis structure has 2.33% (valence non-Lewis, 2.18% and Rydberg non-Lewis, 0.16%) in the studied compound. The NBO results showed that the σ(C1 - C2) bond was formed from the sp$^{1.47}$ hybrid orbital on carbon (59.43% *p*-character) interacting with sp$^{1.96}$ hybrid on carbon (66.15% *p*-character). The sp$^{3.01}$ hybrid on carbon atom (74.94% *p*-character) was interacted with sp$^{4.36}$ hybrid of sulfur atom (80.87% *p*-character) to form σ(C4 – C5) bond. Similarly,

the σ (C13 – N21) bond was formed through the interaction between the sp$^{2.51}$ ybrid on carbon atom (71.43% *p*-character) and the sp$^{1.72}$ hybrid of nitrogen (63.17% *p*-character) (**Table 4**).

The second order perturbation theory analysis of fock matrix basis in NBO analysis between donor and acceptor orbitals of the studied compound are represented in **Table 5**. The nature of interaction between the donor (i) and acceptor (j) is determined by the value of the stabilization energy. The stability of the system increases with increased electron delocalization associated with hyperconjugation, thus, a high stabilization energy [33]. The significant hyperconjugative interactions and the value of their stabilization energies observed from the NBO analysis are: π(C11 – C13) → (C6 – C8) (24.56 Kcal/mol), π(C6 – C8) → π^*(C7 – C9) (23.08 Kcal/mol), π(C7 – C9) → π^*(C11 –C13) (21.37 Kcal/mol), π(C6 – C8) → π^*(C11 – C13) (17.72 Kcal/mol), π(C11 – C13) → π^*(C7 – C9) (16.58 Kcal/mol), π(C7 – C9) → π^*(C6 – C8) (15.71 Kcal/mol), π(C3 – C4) → π^*(C1 – C2) (10.88 Kcal/mol), π(C3 – C4) → π^*(C1 – C2) (6.3 Kcal/mol).

These stabilization energies correspond to the stability of the phenyl ring and the charge transfer within the molecules of the studied compound. The energies for the interaction between LP(2)S5 → π^*(C1 – C2) (24.39 Kcal/mol) and LP(2)S5 → π^*(C3 – C4) (17.39 Kcal/mol) stabilized the structure and proved the resonance between the heteroatom and the phenyl ring of **AI3**.

3.5. Frontier molecular orbital (FMO)

The Frontier Molecular Orbital (FMO) focuses on the highest occupied molecular orbital and the lowest unoccupied molecular orbital, HOMO and LUMO respectively. It is relevant in evaluating the chemical reactivity and the kinetic stability of a molecule. Within the molecule, the HOMO indicates its ability to donate an electron, while the LUMO indicates its electron acceptance ability. The difference between the energy values of the HOMO and the energy values of the LUMO orbitals ($E_{HOMO} - E_{LUMO}$) correspond to the energy gap of the molecule. The energy gap provide details that indicates the structure's stability and intra-molecular interaction as a result of charge transfer between the donor and acceptor atom [34]. The values of the E_{HOMO}, E_{LUMO} and energy gap were computed with GuassView 6 software using the output log file gotten from the optimized structure. The analysis revealed that **AI3** has 247 molecular orbitals, out of which 56 molecular orbitals are occupied. The HOMO were mostly localized on the nitrogen atom, N21 of the amino substituent attached to the phenyl ring and also on the carbon atom, C4 of the thiophene ring. The LUMO were localized on the carbon atom, C1 and partially on the sulfur atom, S5 both on the thiophene ring [35]. The Chemical Hardness (η), Softness (s), Chemical Potential (μ), Electronegativity (χ) and Electrophilicity index (ω) were calculated using the following formula;

Table 5
Second order perturbation theory analysis of Fock matrix basis in NBO analysis between donor and acceptor orbitals of the studied compound.

Donor(i)	Occupancy	Acceptor(j)	Occupancy	$E^{(2)}$ Kcal/mol	E(i) − E(j) (a.u)	F(i,j) (a.u)
σC1-C2	1.96794	σ^*C2-C3	0.03280	3.71	1.24	0.060
		σ^*C19-N20	0.00956	4.26	1.62	0.075
σC2-C19	1.97600	σ^*C1-C2	0.02915	3.26	1.29	0.058
		σ^*C19-N20	0.00956	6.08	1.62	0.089
πC3-C4	1.89480	π^*C1-C2	0.43015	10.88	0.28	0.054
		π^*C6-C8	0.39540	6.32	0.32	0.043
σC4-S5	1.97708	σ^*C1-N16	0.01783	4.63	1.09	0.063
		σ^*C3-C6	0.03138	5.02	1.15	0.068
σC4-H24	1.98370	σ^*C2-C3	0.03280	3.54	1.05	0.055
		σ^*C3-C4	0.02053	2.79	1.15	0.051
σC6-C7	1.97199	σ^*C3-C6	0.03138	2.83	1.17	0.051
		σ^*C6-C8	0.02299	3.56	1.25	0.060
σC6-C8	1.97212	σ^*C3-C6	0.03138	2.76	1.17	0.051
		σ^*C6-C7	0.02262	3.59	1.25	0.060
πC6-C8	1.64752	π^*C7-C9	0.33362	23.08	0.28	0.071
		π^*C11-C13	0.40510	17.72	0.27	0.063
σC7-C9	1.97765	σ^*C3-C6	0.03138	3.29	1.18	0.056
		σ^*C13-N21	0.01808	3.71	1.14	0.058
πC7-C9	1.71920	π^*C6-C8	0.39540	15.71	0.29	0.062
		π^*C11-C13	0.40510	21.37	0.28	0.072
σC7-H10	1.98122	σ^*C6-C8	0.02299	3.91	1.09	0.058
		σ^*C9-C13	0.02287	3.95	1.08	0.058
σC8-C11	1.97720	σ^*C3-C6	0.03138	3.44	1.18	0.057
		σ^*C13-N21	0.01808	3.71	1.13	0.058
σC8-H12	1.97952	σ^*C6-C7	0.02262	3.97	1.09	0.059
		σ^*C11-C13	0.02274	4.02	1.08	0.059
σ(1)C9-C13	1.97422	σ^*C7-C9	0.01242	2.69	1.29	0.053
		σ^*C11-C13	0.02274	3.34	1.26	0.058
πC11-C13	1.62160	π^*C6-C8	0.39540	24.56	0.29	0.075
		π^*C7-C9	0.33362	16.58	0.28	0.062
LP(2)S5	1.68168	π^*C1-C2	0.43015	24.39	0.26	0.073
		π^*C3-C4	0.02053	17.39	0.29	0.063
LP (1)N20	1.96899	RY*(1)C19	0.01929	16.51	1.14	0.123
		σ^*C2-C19	0.03311	12.73	1.05	0.103

LP - Lone pair.
$E^{(2)}$ - Stabilization energy.
E(i) − E(j) - Energy difference between the donor and acceptor NBO orbitals.
F(i,j) - The Fock Matrix element between i and j NBO orbitals.

$$\eta = \frac{I - A}{2} \qquad (3)$$

$$S = \frac{I}{2}\eta \qquad (4)$$

$$\chi = -\mu = \frac{I + A}{2} \qquad (5)$$

$$\omega = \frac{\mu^2}{2}\eta \qquad (6)$$

The Electrophilicity index measures the system's stability when it obtains additional surrounding charge. The electronegativity and chemical potential of the molecule is a property of the whole molecule and they remain constant throughout. The chemical softness reveals the nature of toxicity of the molecule. The low softness value (−0.21701) indicates low toxicity. The value of the energy gap of the HOMO and LUMO (−4.608102) is comparable to those of HOMO-1/LUMO+1 (−5.64202) and the HOMO-2/LUMO+2 (−6.65728). The decreased value of the energy gap of the HOMO and LUMO proves the biological reactivity of the molecule (low stability) and indicates the presence of NLO effects**.** The low value of Chemical hardness proves (−2.30405) that the studied structure is a soft molecule [36,37]. The distributions and energy levels of HOMO-2, HOMO-1, HOMO, LUMO, LUMO+1, LUMO+2 are shown in **Fig. 3**. The **Table 6**. represents the calculated energy values of the studied ligand.

Table 6
Calculated energy values of **AI3** by the B3LYP/6–311++G (d, p) approach.

B3LYP	6–311++G (d,p)
E_{total} (a.u)	−26,857.9527
E_{HOMO} (eV)	−5.251973
E_{LUMO} (eV)	−0.643870
E_{HOMO} - E_{LUMO} gap (eV)	−4.608103
E_{HOMO-1} (eV)	−5.88637
E_{HOMO-2} (eV)	−6.75632
E_{LUMO+1} (eV)	−0.24435
E_{LUMO+2} (eV)	−0.09904
E_{HOMO-1} - E_{LUMO+1} gap (eV)	−5.64202
E_{HOMO-2} - E_{LUMO+2} gap (eV)	−6.65728
Chemical Hardness(η)	−2.30405
Softness (s)	−0.21701
Chemical Potential (μ)	2.94792
Electronegativity (χ)	−2.94792
Electrophilicity index (ω)	−1.88586

3.6. Electrostatic potential (ESP)

The Electrostatic Potential, *ESP* was determined to provide graphical representation of the chemically active sites and the atom reactivity. The analysis of the *ESP* is based on the nature of interaction between the positive regions of the electrostatic potential on a surface with the negative region on the other surface. This reveals the sites susceptible for nucleophilic and electrophilic attack, charge distribution and interaction between hydrogen bond-

LUMO+2
E_{LUMO+2} = -0.09904 eV

LUMO+1
E_{LUMO+1} = -0.24435 eV

LUMO

E_{LUMO} = -0.64387 eV

E_{HOMO} - E_{LUMO} = -4.608103 eV

E_{HOMO-1} - E_{LUMO+1} = -5.64202 eV

E_{HOMO-2} - E_{LUMO+2} gap = -6.65728 eV

E_{HOMO} = -5.251973

HOMO

HOMO-1
E_{HOMO-1} = -5.88637 eV

HOMO-2
E_{HOMO-2} = -6.75632 eV
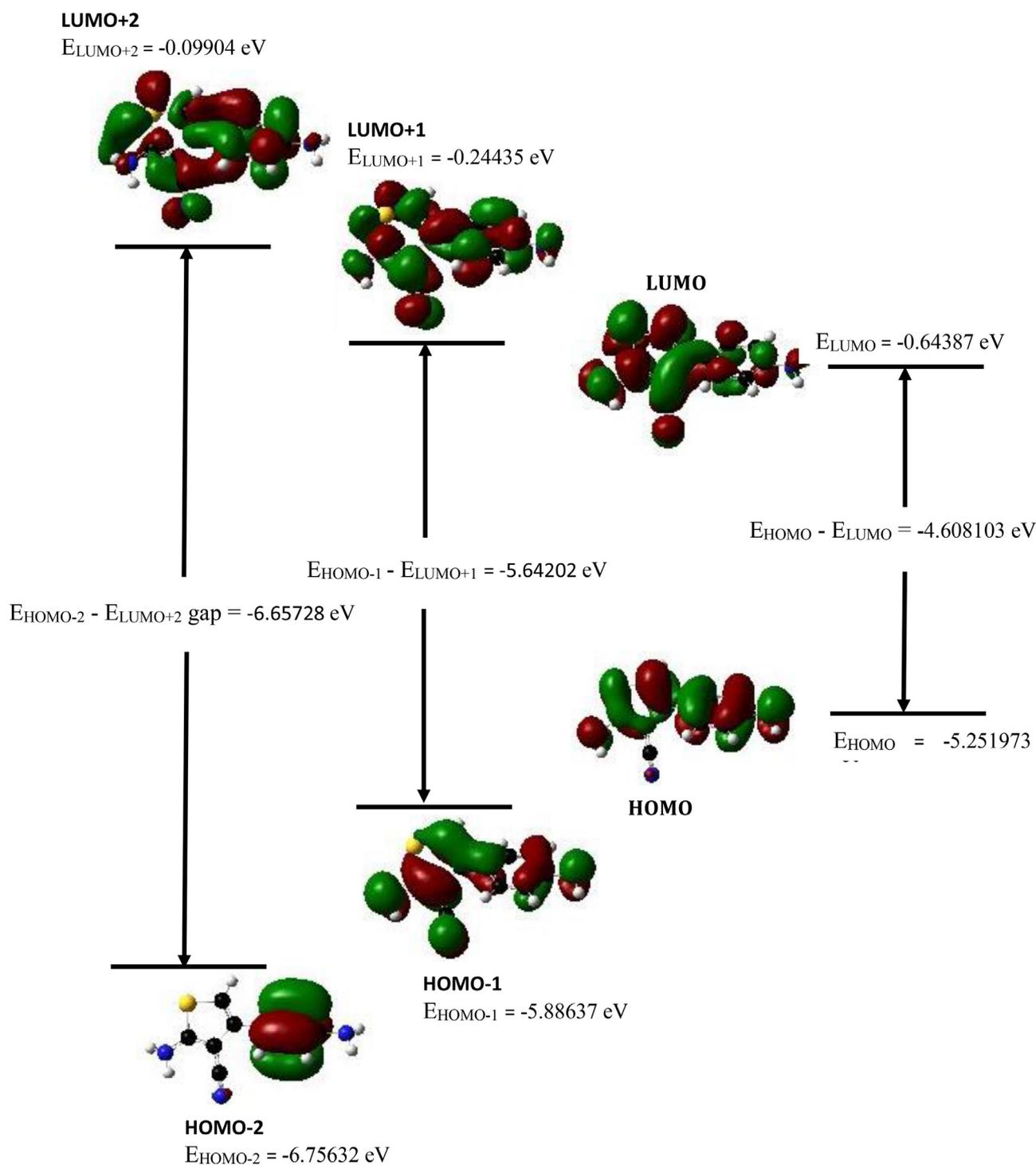
Fig. 3. Molecular Orbital Surfaces and Energy Levels highlighted for the HOMO-2, HOMO-1,HOMO, LUMO+1, LUMO+2 and LUMO of the ligand in view at the B3LYP/6−311++ *G* (d,p) level.

ing [38]. The more the electropositivity and electronegativity, the stronger the tendency for *ESP*. **Fig. 4.** represents the isosurface plot for the title compound. The red and blue spheres represent surface local minima and maxima of ESP respectively. The red sphere represents the region with high electron dominance and it is identified with their negative isosurface values while the blue sphere corresponds to the region with electron deficiency and can also be identified with their positive isosurface values. The highest minimum on the surface of the studied compound was located at S5 (−0.001 Kcal/mol), this is due to the tendency of the Sulfur to at-

tract electrons as an electronegative atom. The highest maxima on the surface of the compound was found at N16 (0.029 Kcal/mol) and this is due to charge differences between surrounding H atoms and carbonyl carbon atom.

3.7. Non linear optical analysis

In an applied electric field, the response of a system is determined by the polarizabilities and hyperpolarizabilities [39]. They define the Non Linear Optic (NLO) properties of the system and
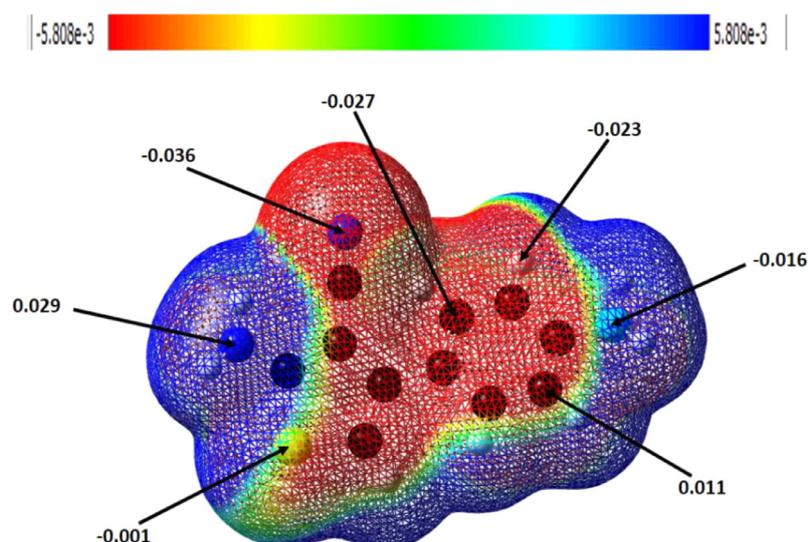
Fig. 4. ESP Isosurface plot studied with DFT/B3LYP method and 6–311++G (d,p) basis set. (For interpretation of the references to color in this figure, the reader is referred to the web version of this article.)

the strength of molecular interactions including the cross sections of several scattering and collision properties [40]. The NLO activity emerges from optical switching, frequency shifting and optical memory. Nonlinear optics is a logical technique for imaging drug delivery. It is also used in biomedical settings to image drug molecules and various particles in cell cultures and tissue samples [41]. The first order hyperpolarizability and the polarizabilities of **AI3** was calculated using *B3LYP/6–311++G (d,p)* method. Although, the α and β values gotten from the NLO output file from Guassian were initially given in atomic units (a.u), however in this study, the results were converted into electronic units (esu), (for α; 1 a.$u = 0.1482 \times 10^{-24}$ esu) and (for β; 1 a.$u = 8.6393 \times 10^{-23}$ esu).

The mean first order hyper polarizability value, (β_{tot}) is 2.251×10^{-29} esu. The maximum value of the dipole moment, (μ_z) along the z direction is -2.03337 Debye. The mean polarizability (α_{tot}) and the anisotropy of the polarizability (Δ_α) equals 2.268×10^{-23} esu and 2.596×10^{-23} esu respectively. Urea is one of the prototypical molecules used in the study of the NLO properties of molecular systems and as a reference molecule for comparative purposes. The studied compound calculated dipole moment and mean first order polarizability is greater than that of urea (The dipole moment 1.5256 Debye and first order hyper polarizability is 0.7803×10^{-30} esu) obtained by *B3LYP/6–311++G (d,p)* method [42]. These results indicate that **AI3** is a good candidate of NLO material.

The mean first order hyperpolarizability(β_{tot}), total dipole moment (μ), the mean polarizability (α_{tot}) and the anisotropy of the polarizability (Δ_α) were calculated using the following equations. The obtained values are represented in **Table S8** of the supporting information.

$$\beta_x = \beta_{xxx} + \beta_{xyy} + \beta_{xzz} \tag{7}$$

$$\beta_y = \beta_{yyy} + \beta_{xxy} + \beta_{yzz} \tag{8}$$

$$\beta_z = \beta_{zzz} + \beta_{xxz} + \beta_{yyz} \tag{9}$$

$$\beta_{total} = \sqrt{\left(\beta_x^2 + \beta_y^2 + \beta_z^2\right)} \tag{10}$$

$$\mu = \sqrt{\left(\mu_x^2 + \mu_y^2 + \mu_z^2\right)} \tag{11}$$

$$\alpha_{total} = \frac{(\alpha_{xx} + \alpha_{yy} + \alpha_{zz})}{3} \tag{12}$$

$$\Delta_\alpha = \sqrt{\left((\alpha_{xx} - \alpha_{yy})^2 + (\alpha_{yy} - \alpha_{zz})^2 + (\alpha_{zz} - \alpha_{xx})^2\right)} \tag{13}$$

3.8. Drug likeness and ADMET analysis

Drug likeness is a balance of various structural and molecular properties tested for effective and efficient results to aid drug discovery and production. Also accessed are the absorption, distribution, metabolism, excretion and toxicity (ADMET) properties of the compound. In this study, drug likeness and ADMET properties of the studied compound were investigated and the predicted results are compiled in Table 7**.** The drug likeness of the compound is accessed based on the Lipinski's rule of five (RO5) and the result shows no violation of the rule. The physicochemical parameters with their ranges as defined by the Lipinski's rule of five include; Molecular weight <500, Hydrogen bond donor ≤ 5, Hydrogen bond acceptor ≤ 10, High lipophilicity log$P$ <5.

The ADMET results presented in **Table 8.** indicate that the compound has excellent absorption due to its promising solubility and permeability [43]. The Human Intestinal Absorption (HIA) is an important requirement for the apparent efficacy of an oral drug [44]. The result shows good absorption at 89.51%. Skin permeability is considered in transdermal drug delivery and evaluates product efficacy, the studied compound shows low skin permeability at -3.225. Blood-brain barrier (BBB) permeability is essential for drugs that are targeted to penetrate the brain. High values of the BBB permeability of drugs not targeted to penetrate the brain leads to unwanted central nervous system CNS related side effects [45]. The studied compound possesses a low BBB penetration value at logBB -0.02 and a considerably high CNS value at logPS -1.962 and can thus penetrate the brain. CYP1A2 is an isoform of Cytochrome P450 inhibitor found in the liver as a detoxification enzyme in the body and the study indicates its presence in the compound [46]. Consequently, **AI3** has shown fair toxicity profile based on the toxicity risk assessment. The AMES toxicity is an assessment for mutagenicity [47] and the compound is predicted to be AMES positive. However, the compound is predicted to have a high estimate of toxic dose threshold (Maximum Tolerated Dose, MTD) of chemicals in humans at 0.621 (log mg/kg/day) [48]. Hepatotoxicity

Table 7

Molinspiration property values for 2-amino-4-(4-aminophenyl)thiophene-3-carbonitrile.

mi LogP	TPSA	n atoms	Molecular weight	No. of H-bond acceptors	No. of H-bond donor	No. of Violations	volume	n rotb
1.69	75.84	15	215.28	4	3	0	185.60	1

Logarithm of partition coefficient (miLogP).
Topological polar surface area (TPSA).
Molecular weight (MW).
Number of rotatable bonds (n-rotb).

Table 8

ADMET Properties of 2-amino-4-(4-aminophenyl)thiophene-3-carbonitrile.

Absorption	Water solubility	−2.884	Numeric (log mol/L)
	Caco2 permeability	0.86	Numeric (log Papp in 10^{-6} cm/s)
	Human Intestinal absorption	89.51	Numeric (% Absorbed)
	Skin Permeability	−3.225	Numeric (log Kp)
	P-glycoprotein substrate	Yes	Categorical (Yes/No)
Distribution	Fraction unbound (human)	0.158	Numeric (Fu)
	BBB permeability	−0.02	Numeric (log BB)
	CNS permeability	−1.962	Numeric (log PS)
Metabolism	CYP1A2 inhibitior	Yes	Categorical (Yes/No)
Excretion	Total Clearance	0.015	Numeric (log ml/min/kg)
	Renal OCT2 substrate	Yes	Categorical (Yes/No)
Toxicity	AMES toxicity	Yes	Categorical (Yes/No)
	Max. tolerated dose (human)	0.621	Numeric (log mg/kg/day)
	hERG I inhibitor	No	Categorical (Yes/No)
	hERG II inhibitor	No	Categorical (Yes/No)
	Oral Rat Acute Toxicity (LD50)	2.55	Numeric (mol/kg)
	Oral Rat Chronic Toxicity (LOAEL)	1.06	Numeric (log mg/kg_bw/day)
	Hepatotoxicity	No	Categorical (Yes/No)
	Skin Sensitization	No	Categorical (Yes/No)
	T.Pyriformis toxicity	0.865	Numeric (log ug/L)
	Minnow toxicity	1.061	Numeric (log mM)

signals drug-induced liver impairments and leads to the discontinuation of drug production when present [49], interestingly, the study records its absence. Skin sensitization is a safety assessment indicator that provides information on a compound's ability to induce skin allergy when administered [50] and the result proves that the compound is safe and unable to cause allergies on the skin.

3.9. Molecular docking

Molecular docking is an essential technique employed in the study of the binding interactions between target proteins and ligands (small molecules). It is useful in the virtual screening of drug-like molecules and the determination of the binding conformations and affinities of the ligand to the protein, thereby resulting in the advancement of drug development [9]. Three (3) *Mycobacterium tuberculosis* proteins with *Escherichia coli* as their expression system, 1P44, 1P45 and 4TZK were chosen to study the antitubercular property of the ligand. The target proteins (.pdb format) were downloaded from RCSB (Research Collaboratory for Structural Bioinformatics) protein data bank (http://www.rcsb.org). The graphical user interface of Autodock Tools-1.5.6 [51] was used to prepare the proteins through the removal of water, defining and editing of binding sites, the addition of polar hydrogens as well as required charges. The ligand was optimized to minimum energy at *B3LYP/6–311++G (d,p)* basis set using Guassian 09 w. The protein-ligand interactions were analyzed using the Discovery Studio 2020 Client to give the molecular binding mode, the 2-D ligand-protein interaction and the Ramachandran plot. The docking conformation with the lowest binding energy was selected to study the mode of binding . The lower the binding affinity, the stronger the ligand binds to the protein. The molecular binding mode of the 3 target proteins (1P44, 1P45 and 4TZK) are represented in **Figs. 5 a**, **6 a** and **7 a** respectively. The 2-dimensional representation of the ligand-protein interaction with highlighted binding sites and bond distance are shown in **Figs. 5b**, **6b** and **7b**, while **7c, 8c** and **9c** showcases the Ramachandran plots respectively for 1P44, 1P45 and 4TZK.

3.9.1. Protein

The ligands-1P44 protein complexes were stabilized by hydrogen bonds, $\pi - sigma$, van der Waals, $\pi - alkyl$, amide- π stacked interactions. In **AI3–1P44** complex, four hydrogen bonds were formed between residues LYS57, ASP223 at the distance, 2.56522, 3.03077, 2.6642 and 2.48023, respectively. The six membered ring and the five membered ring of residue PRO59, ALA58 and LYS57 interacted to form three hydrophobic interactions at a distance, 3.52585, 4.87192 and 5.15397, respectively.

For the **ISONIAZID-1P44** complex, six hydrogen bonds were formed between residues GLN49, LYS181, ALA58 and ALA56 at the distance, 2.43983, 2.2281, 2.33417, 2.41012, 2.35067 and 3.60909. One electrostatic interaction was formed at 3.37332 with residue ASP52 while two hydrophobic interactions were formed with residues LYS57, LYS181 at 4.80331 and 4.77031.

3.9.2. Protein

The ligands-1P45 protein complexes were stabilized by hydrogen bonds, van der Waals, $\pi - anion$ and electrostatic interactions. As observed from the **AI3–1P44** complex, five hydrogen bond interactions were found with residues SER166, ARG173 and SER152 at the distance, 2.52214, 2.20941, 1.79445, 2.39001 and 2.31237. At ARG173 residue, an electrostatic bond with $\pi - cation$ and $\pi -$ donor hydrogen bond interaction is formed at a distance, 3.80185.

At the bond distance, 3.0581, 1.75795, 1.97199, 2.44965 and 2.20891, five hydrogen bonds were formed were found in the residues SER166, ARG173, GLU169. Also, an electrostatic $\pi - anion$ interaction is observed in the residue GLU169 due to the interaction between the 1P45 protein and the standard drug, **ISONIAZID** (**Fig. 6a** and **b**).
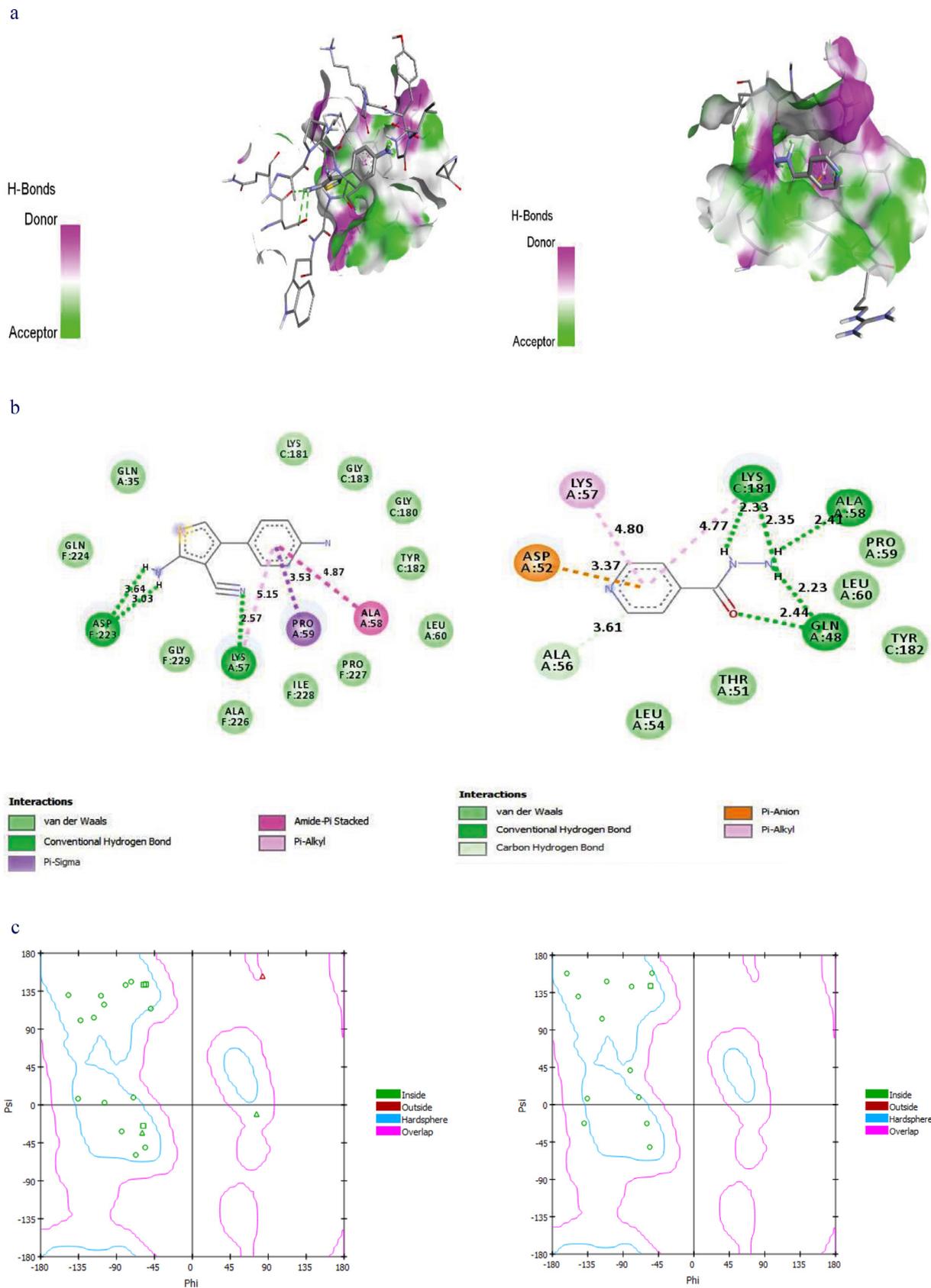
Fig. 5. (a): Binding mode of **AI3** and **ISONIAZID** at the binding site of 1P44. (b). 2-D ligand-protein (1P44) interaction. (c). Ramachandran plot: 1P44 interaction.
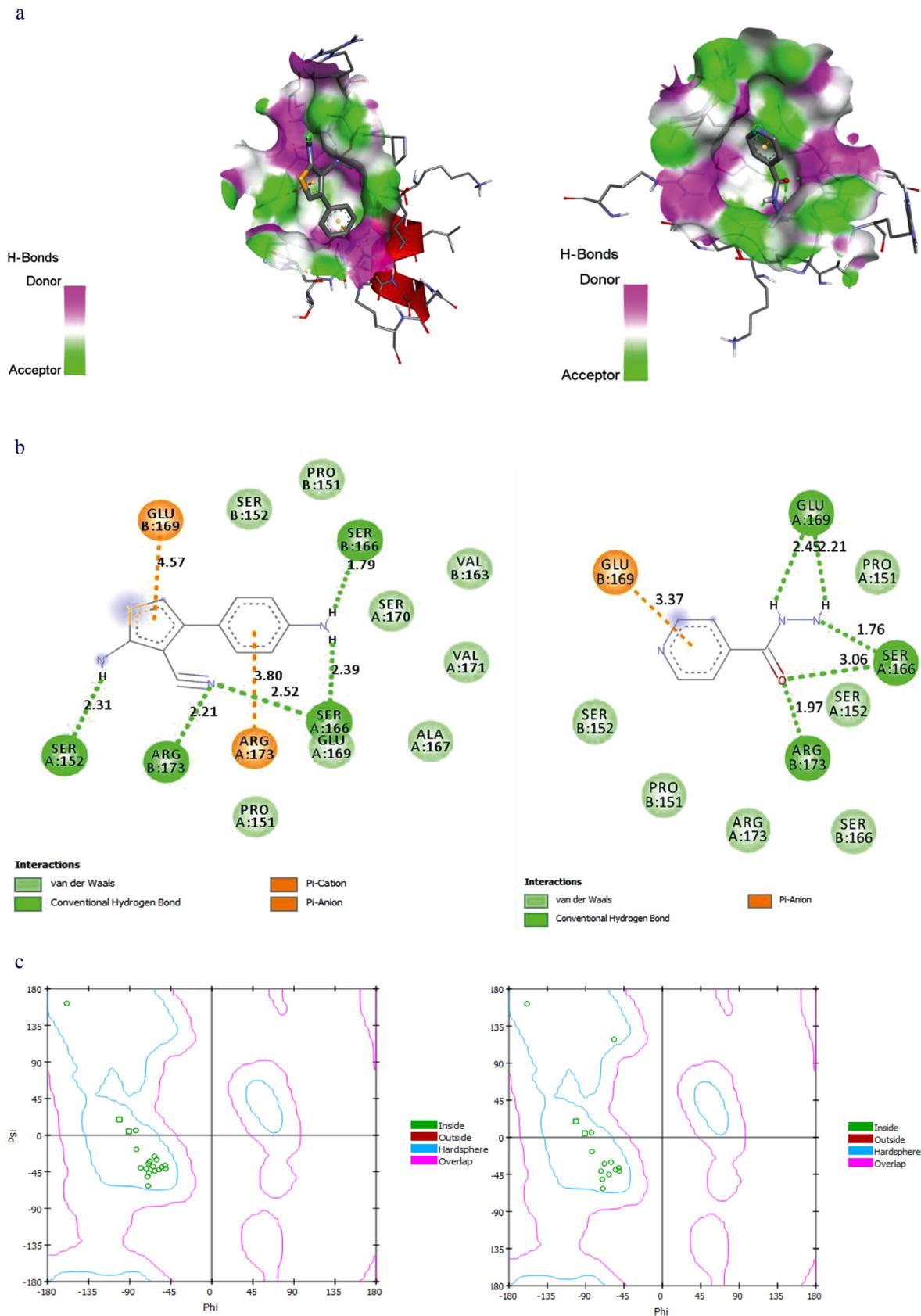
Fig. 6. (a). Binding Mode of **AI3** and **ISONIAZID** at the binding site of 1P45. (b). 2-D ligand-protein (1P45) interaction. (8). Ramachandran plot: 1P45 interaction.
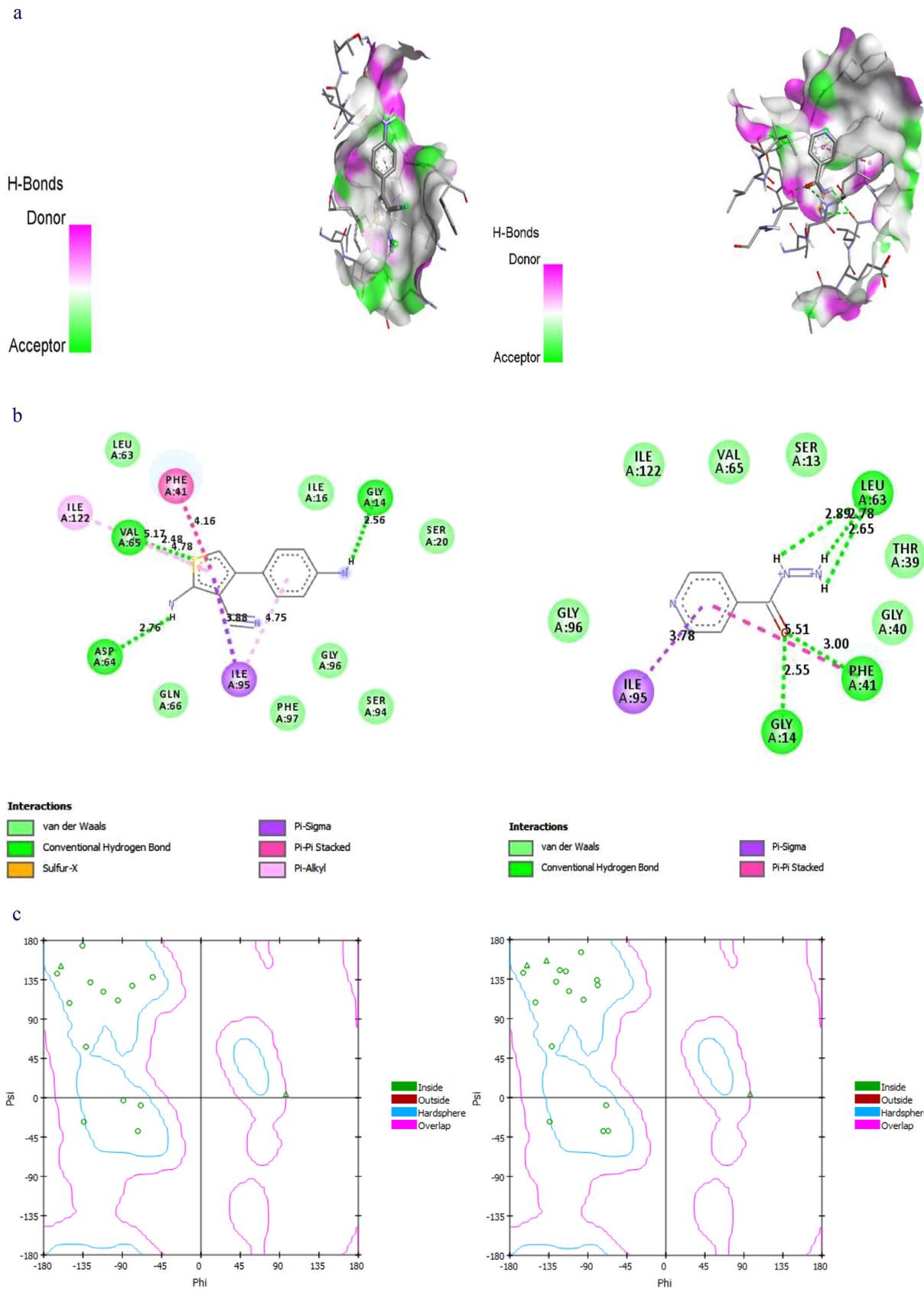
Fig. 7. (a). Binding Mode of **AI3** and **ISONIAZID** at the binding site of 4TZK. (9). 2-D ligand-protein (4TZK) interaction. (c). Ramachandran plot: 4TZK interaction.

3.9.3. Protein

Consequently, the ligand-4TZK protein complexes consist of hydrogen bonds $\pi - sigma$, van der Waals, $\pi - alkyl$, $\pi - \pi$ interactions which stabilize the complexes. In the **AI3–4TZK** complex, the residues VAL65, GLY14 and ASP64 formed three hydrogen bonds at the distance, 2.48461, 2.56224 and 2.75665. A sulfur-X bond formed at the distance, 3.33036 was found in the residue VAL65. A hydrophobic $\pi - sigma$ interaction is observed at a distance 3.88393 in the ILE95 residue. At the distance, 4.15898, in the PHE41 residue, a hydrophobic $\pi - \pi$ interaction is noticed. Furthermore, three hydrophobic $\pi - alkyl$ interactions were found in the ILE95, VAL65, ILE122 residues at 4.755, 4.77925 and 5.16583, respectively.

In the **ISONIAZID-4TZK** complex, five hydrogen bonds were formed at 2.54798, 3.00409, 2.88614, 2.78222 and 2.65371 with residues GLY14, PHE41, LEU63. One $\pi - sigma$ hydrophobic interaction was observed in the residue ILE95 at the distance 3.7812. Also, one $\pi - \pi$ hydrophobic interaction was observed in PHE41 at 5.51148. (Fig. 7a and **b**)

The trend in the binding energies, hydrogen bonds and hydrophobic contacts of the studied ligand, the standard drug with the target proteins are highlighted in **Tables S11** and **S12.** of the supporting information. In drug discovery, the binding affinities provide details that aid drugs bind their targets selectively and specifically. The docked **AI3 complexes** has comparatively better binding affinities (-6.0, -3.9 and **-7.2** kcal/mol) than the complexes of the standard drug, **ISONIAZID** (-5.5, -3.8 and -5.6 kcal/mol) for respective target proteins. Also, both complexes have comparative observable hydrogen bonds which are vital in the structure and function of biological processes. Therefore, this proves the suitability of **AI3** as a potential anti-tubercular drug.

4. Conclusion

The results obtained show good agreements between the experimental and theoretical spectroscopic analysis of 2-amino-4-(4-aminophenyl)thiophene-3-carbonitrile. Utilizing the *DFT/B3LYP* method with *6–311++G (d,p)* basis set, the optimized geometry, vibrational frequencies, atomic charges, chemical reactivity parameters, natural bond orbital and the non-linear optical effects were calculated and reported. The energy gap calculated from the HOMO/LUMO has a lower value of -4.608103 eV and thus, indicates the presence of NLO effect, low kinetic stability and the high biological activity of the studied compound. The result of the non linear optical analysis, showcased the compound to be a good candidate of NLO material. The molecular docking result suggests that the compound might exhibit antitubercular effects against *Mycobacterium tuberculosis* as a better binding energy of **AI3** was reported in comparison to that of a standard antitubercular drug, Isoniazid.[52] The result of the ADMET analysis also proves good drug likeness and excellent ADME properties as well as permissible toxicity assessment. Hence, we hope our research will serve as a useful guide for further studies and synthesis of 2-amino-4-(4-aminophenyl)thiophene-3-carbonitrile.

Declaration of Competing Interest

The authors declare no competing financial interest.

CRediT authorship contribution statement

Queen S. Obu: Formal analysis, Writing – original draft, Investigation. **Hitler Louis:** Conceptualization, Visualization, Supervision, Resources. **Joseph O. Odey:** Investigation, Validation. **Ishegbe Joyce Eko:** Methodology. **Shuaibu Abdullahi:** Data curation. **Tabe N. Ntui:** Writing – review & editing. **Ofiong E. Offiong:** Conceptualization, Supervision, Writing – review & editing.

References

[1] S. Pathania, R. Kumar Narang, R.K. Rawal, Role of sulphur-heterocycles in medicinal chemistry: An update., Eur. J. Med. Chem. 180 (2019) 486–508.

[2] M. Feng, B. Chang, Y. Li, X. Zhang, H. Li, Pyridinium 1, 4-zwitterionic thiolates as a useful class of sulfur-containing synthons: application to the synthesis of 2, 5-dihydro-1, 4, 5-thiadiazepines, Chemical Communications 55 (2019) 14606–14606.

[3] L. Schutte, R. Teranishi, Precursors of sulfur-containing flavor compounds., Crit. Rev. Food Sci. Nutr. 4 (1974) 457–505.

[4] P.H. Wang, H.F. Lee, Y.C. Huang, Y.J. Jung, F.L. Gong, W.Y. Huang, The proton dissociation constant of additive effect on self-assembly of poly (3-hexyl-thiophene) for organic solar cells., Electron Mater. Lett. 10 (2014) 767–773.

[5] Y. Tian, X. Wei, H. Xu, Photoactivated Insecticidal Thiophene Derivatives from Xanthopappus s ubacaulis., J. Nat. Prod. 69 (2006) 1241–1244.

[6] M. Helal, M. Salem, M. Gouda, N. Ahmed, A. El-Sherif, Design, synthesis, characterization, quantum-chemical calculations and anti-inflammatory activity of novel series of thiophene derivatives., Spectrochim. Acta A Mol. Biomol. Spectrosc. 147 (2015) 73–83.

[7] WHOGlobal Tuberculosis Report 2019, 2020 Tuberculosis[online] https://www.who.int/teams/global-tuberculosis-programme/tb-reports/global-tuberculosis-report-2020 (Accessed January 17, 2020).

[8] S.A. Shipilovskikh, V.Y. Vaganov, R.R. Makhmudov, A.E. Rubtsov, Synthesis and Antinociceptive Activity of N-Substituted 4-Aryl-4-oxo-2-[(3-thiophen-2-yl) amino] but-2-enamides., Russ. J. Gen. Chem. 4 (2020) 583–589.

[9] C.B. Pradeep Kumar, M.S. Raghu, K.N.N. Prasad, S. Chandrasekhar, B.K. Jayanna, dfA. Alharthi, M.K. Prashanth, K. Yogesh Kumar, Investigation of biological activity of 2, 3-disubstituted quinazolin-4 (1 H)-ones against Mycobacterium tuberculosis and DNA via docking, spectroscopy and DFT studies., New J. Chem. 45 (2021) 403–414.

[10] R. Haunschild, A. Barth, B. French, A comprehensive analysis of the history of DFT based on the bibliometric method RPYS., J. Cheminform. 11 (2019) 1–15.

[11] S. Naseem, M. Khalid, M.N. Tahir, M.A. Halim, A.A.C. Braga, M.M. Naseer, Z. Shafiq, Synthesis, structural, DFT studies, docking and antibacterial activity of a xanthene based hydrazone ligand., J. Mol. Struct. 1143 (2017) 235–244.

[12] M.D. Hanwell, D.E. Curtis, D.C. Lonie, T. Vandermeersch, E. Zurek, G.R. Hutchison, Avogadro: an advanced semantic chemical editor, visualization, and analysis platform., J. Cheminform. (2012) 4–17.

[13] A.D. Becke, J. Chem. Phys. 98 (1993) 5648–5652; A.D. Becke, J. Chem. Phys. 98 (1993) 1372–1377.

[14] M.J. Frisch, G.W. Trucks, H.B. Schlegel, G.E. Scuseria, M.A. Robb, J.R. Cheeseman, G. Scalmani, V. Barone, B. Mennucci, G.A. Petersson, H. Nakatsuji, M. Caricato, X. Li, H.P. Hratchian, A.F. Izmaylov, J. Bloino, G. Zheng, J.L. Sonnenberg, M. Hada, M. Ehara, K. Toyota, R. Fukuda, J. Hasegawa, M. Ishida, T. Nakajima, Y. Honda, O. Kitao, H. Nakai, T. Vreven, J.A. Montgomery, J.E. Peralta, F. Ogliaro, M. Bearpark, J.J. Heyd, E. Brothers, K.N. Kudin, V.N. Staroverov, R. Kobayashi, J. Normand, K. Raghavachari, A. Rendell, J.C. Burant, S.S. Iyengar, J. Tomasi, M. Cossi, N. Rega, J.M. Millam, M. Klene, J.E. Knox, J.B. Cross, V. Bakken, C. Adamo, J. Jaramillo, R. Gomperts, R.E. Stratmann, O. Yazyev, A.J. Austin, R. Cammi, C. Pomelli, J.W. Ochterski, R.L. Martin, K. Morokuma, V.G. Zakrzewski, G.A. Voth, P. Salvador, J.J. Dannenberg, S. Dapprich, A.D. Daniels, Ö. Farkas, J.B. Foresman, J.V. Ortiz, J. Cioslowski, D.J. Fox, Gaussian 09, revision C. 02 Gaussian, Inc., Wallingford CT 2009.

[15] M.H. Jomroz, Vibrational energy distribution analysis, VEDA4, Warsaw, 2004.

[16] T. Lu, F. Chen, Multiwfn: a multifunctional wafefunction analyzer, J. Comput. Chem. 33 (2012) 580.

[17] J. Sánchez-Márquez, D. Zorrilla, A. Sánchez-Coronilla, M. Desireé, J. Navas, C. Fernández-Lorenzo, J. Martín-Calleja, Introducing "UCA-FUKUI" software: reactivity-index calculations, Journal of molecular modeling 20 (11) (2014) 1–13.

[18] R. Dennington, T. Keith and J. Milam, Gauss View, Version 5, Semichem Inc., Shawnee Mission KS 2009.

[19] Molinspiration Cheminformatics https://molinspiration.com/

[20] pkcSM- Pharmacokineics http://biosig.unimelb.edu.au/pkcsm/prediction

[21] O. Trott, A.J. Olson, AutoDock Vina: improving the speed and accuracy of docking with a new scoring function, efficient optimization, and multithreading., J. Comput. Chem. 31 (2010) 455–461.

[22] A.A. Bunaciu, H.Y. Aboul-Enein, V.D. Hoang, Vibrational micro-spectroscopy of human tissues analysis., Trends Analyt. Chem. 68 (2015) 14–22.

[23] I. Azad, A. Yusuf, K. Tahmeena, I.A. Mohammad, C. Subhash, S. Praveer, K. Durgesh, N. Malik, Synthesis, structural characterization and computational study of a novel amino chalcone: a potential nonlinear optical material., J. Mol. Struct. 1203 (2020) 0022–2860.

[24] D.L. Pavia, G.M. Lampman, G.S. Kriz, Introduction to Spectroscopy: A guide For Students of Organic Chemistry, W. B. Saunders Co, Philadelphia, 1979.

[25] N. Ozdemir, R. Kagıt, O. Dayan, Synthesis, structural characterization and computational study of a novel amino chalcone: a potential nonlinear optical material., Mol. Phys. 114 (2016) 757–768.

[26] M.A. Mumit, T.K. Pal, M.A. Alam, M.A. Islam, S. Paul, M.C. Sheikh, DFT studies on vibrational and electronic spectra, HOMO–LUMO, MEP, HOMA, NBO and molecular docking analysis of benzyl-3-N-(2, 4, 5-trimethoxyphenylmethylene) hydrazinecarbodithioate., J. Mol. Struct. 1220 (2020) 0022–2860.

[27] M. Pandy, S. Muthu, N. Gowda, Quantum mechanical and spectroscopic (FT-IR, FT-Raman, 1H, 13C NMR, UV-Vis) studies, NBO, NLO, HOMO, LUMO and Fukui function analysis of 5-Methoxy-1H-benzo [d] imidazole-2 (3H)-thione by DFT studies., Can. J. Chem. 1130 (2017) 511–521.

[28] P. Agrawal, NMR Spectroscopy in Drug Discovery and Development. Mater., Mater. Methods 4 (2014) 599.

[29] Z. Demircioglu, C. Kastas, O. Buyukgungor, Theoretical analysis (NBO, NPA, Mulliken Population Method) and molecular orbital studies (hardness, chemical potential, electrophilicity and Fukui function analysis) of (E)-2-((4-hydroxy-2-methylphenylimino) methyl)-3-methoxyphenol., Indian J. Chem. 1091 (2015) 183–195.

[30] M. Christophe, G. Andre, T.L. Alejandro, New dual descriptor for chemical reactivity., J. Phys. Chem. 109 (2005) 205–212.

[31] R.P. Gangadharan, Natural Bond Orbital (NBO) Population Analysis of 1-Azanapthalene-8-ol., Acta Phys. Pol. 125 (2014) 18–22.

[32] R. Bhuvaneswari, M.D. Bharathi, G. Anbalagan, G. Chakkaravarthi, K.S. Murugesan, Molecular structure, vibrational spectroscopic (FT-IR, FT-Raman), NBO, HOMO and LUMO analysis of morpholinium oxalate by density functional method., J. Mol. Struct. 1173 (2018) 188–195.

[33] E.A. Bisong, H. Louis, T.O. Unimuke, J.O. Odey, E.I. Ubana, M.M. Edim, F.T. Timothy, J.A. Agwupuye, P.M. Utsu, Vibrational, electronic, spectroscopic properties, and NBO analysis of p-xylene, 3, 6-difluoro-p-xylene, 3, 6-dichloro-p-xylene and 3, 6-dibromo-pxylene: A DFT Study, J. Heliyon 12 (2020) 2405–8440.

[34] S. Murugavel, S. Sundramoorthy, D. Lakshmanan, R. Subashini, P.P. Kumar, Synthesis, crystal structure analysis, spectral (NMR, FT-IR, FT-Raman and UV–Vis) investigations, molecular docking studies, antimicrobial studies and quantum chemical calculations of a novel 4-chloro-8-methoxyquinoline-2 (1H)-one: an effective antimicrobial agent and an inhibition of DNA gyrase and lanosterol-14α-demethylase enzymes., J. Mol. Struct. 16 (2016) 0022–2860.

[35] T. Lu, F. Chen, Multiwfn: a multifunctional wavefunction analyzer., Acta Chim. Sin. 69 (2011) 2393–2406.

[36] S. Alyar, S. Tülin, Synthesis, spectroscopic characterizations, enzyme inhibition, molecular docking study and DFT calculations of new Schiff bases of sulfa drugs., J. Mol. Struct. 1185 (2019) 416–424.

[37] G. Banuppriya, R. Sribalan, V. Padmini, Synthesis and characterization of curcumin-sulfonamide hybrids: biological evaluation and molecular docking studies., J. Mol. Struct. 1155 (2018) 90–100.

[38] P.C. Rathi, R.F. Ludlow, M.L. Verdonk, Practical high-quality electrostatic potential surfaces for drug discovery using a graph-convolutional deep neural network., J. Med. Chem. 63 (16) (2020) 8778–8790.

[39] D. Gajalakshmi, M.S. Boobalan, R.V. Solomon, V. Tamilmani, Are vinyl coupled furan derivatives better than vinyl coupled thiophene derivatives for optoelectronic applications?–Answers from DFT/TDDFT calculations., J.Commatsci. 162 (2019) 60–68.

[40] P. Manjusha, J.C. Prasana, S. Muthu, B.F. Rizwana, Spectroscopic elucidation (FT-IR, FT-Raman and UV-visible) with NBO, NLO, ELF, LOL, drug likeness and molecular docking analysis on 1-(2-ethylsulfonylethyl)-2-methyl-5-nitro-imidazole: An antiprotozoal agent., J.Compbiolchem. 88 (2020) 1476–9271.

[41] A.L. Fussell, A. Isomaki, C.J. Strachan, M. Windbergs, H.L. Offerhaus, Nonlinear optical imaging–Introduction and pharmaceutical applications., Am. Pharmaceut. Rev 16 (2013) 54–63.

[42] S. Ramalingama, M. Karabacak, S. Periandy, N. Puviarasan, Spectroscopic (infrared, Raman, UV and NMR) analysis, Gaussian hybrid computational investigation (MEP maps/HOMO and LUMO) on cyclohexanone oxime., Spectrochim. Acta A 94 (2012) 318–330.

[43] L.M. Nainwal, M Shaququzzaman, M Akhter, A Hussain, S Parvez, F Khan, M.M Alam, et al., Synthesis, ADMET prediction and reverse screening study of 3, 4, 5-trimethoxy phenyl ring pendant sulfur-containing cyanopyrimidine derivatives as promising apoptosis inducing anticancer agents, Bioorganic Chemistry 104 (2003) 104282–104282.

[44] R. Kumar, M.H Siddiqui, R.K. Tiwari, et al., Prediction of human intestinal absorption of compounds using artificial intelligence techniques., Current drug discovery technologies 14 (2017) 244–254.

[45] U. Norinder, M. Haeberlein, Computational approaches to the prediction of the blood–brain distribution., Adv. Drug Deliv. Rev. 54 (2002) 291–313.

[46] W.W. Huber, W. Rossmanith, M. Grusch, E Haslinger, . Effects of coffee and its chemopreventive components kahweol and cafestol on cytochrome P450 and sulfotransferase in rat liver., Food and Chemical toxicology 46 (2008) 1230–1238.

[47] W. Wang, D. Zhang, C. Xu, Y. Wu, H. Duan, S. Li, Q. Tan, et al., Heritability and genome-wide association analyses of serum uric acid in middle and old-aged chinese twins., Frontiers in endocrinology 9 (2018) 75–75.

[48] D.S. Cao, et al., In silico toxicity prediction of chemicals from EPA toxicity database by kernel fusion-based support vector machines., Chemom. Intell. Lab. Syst. 146 (2015) 494–502.

[49] F. Ballet, Hepatotoxicity in drug development: detection, significance and solutions., J. Hepatol. 26 (1997) 26–36.

[50] V.M. Alves, et al., Predicting chemically-induced skin reactions. Part II: QSAR models of skin permeability and the relationships between skin permeability and skin sensitization., Toxicol. Appl. Pharmacol. 284 (2015) 262–272.

[51] O. Trott, A.J. Olson, A.D. Vina, AutoDock Vina: improving the speed and accuracy of docking with a new scoring function, efficient optimization, and multithreading., J. Comp. Chem. 31 (2010) 455–461.